Dataset from long-term wind and acceleration monitoring of the Hardanger Bridge

Aksel Fenerci[a1], Knut Andreas Kvåle[a2], Øyvind Wiig Petersen[a3], Anders Rønnquist[a4], Ole Øiseth[a5]

[a]Department of Structural Engineering, Norwegian University of Science and Technology, Trondheim, Norway

Abstract

A large dataset of wind and acceleration data collected through long-term monitoring of the Hardanger Bridge in Norway is described in this data paper. The dataset includes both the raw data and the organized data, and it is published in an open access data repository and therefore can be accessed and downloaded freely. Here, the monitoring system used to acquire the data and the bridge is described first. Then, the methods of signal processing and data adjusting are addressed. Finally, the organization of the dataset is described, and the contents are summarized.

1. Introduction

The need for structural health monitoring of critical infrastructure is well recognized in the structural engineering community. Almost all prominent long-span bridges in the world are equipped with monitoring systems with varying degrees of sophistication. The data that are collected through such monitoring efforts are typically used by the bridge owner or the research community in a wide range of applications. In recent years, knowledge gained through such applications has been frequently communicated among structural engineers through prominent journals and conferences in the field. However, it is also important that the data from these monitoring efforts are made available to the structural engineering community. Here, we present such a dataset from the Hardanger Bridge in Norway, that is available for download and use under a creative commons license.

The wind speeds and accelerations along the main girder of the Hardanger Bridge has been monitored by the Norwegian University of Science and Technology since 2013, and the collected data has been the subject of several research papers on different topics, for instance wind field modeling in complex terrain (Fenerci and Øiseth, 2018), wind-induced response analysis (Lystad et al., 2020), system and force identification (Petersen et al., 2020) and finite element model updating (Petersen and Øiseth, 2017), and others (Fenerci et al., 2017; Fenerci and Øiseth, 2018; Fenerci and Øiseth, 2017a, 2017b, 2017c; Lystad et al., 2019, 2018; Petersen et al., 2019, 2017). However, it is expected that the long-term data presented here can be useful in a variety of different structural engineering applications. Validation of wind/turbulence models or computational fluid dynamics simulations, operational modal analysis, force and system identification of bridges can be named as a few examples; however, the list can certainly be extended.

The paper is organized as follows: In section 2, the monitoring campaign is introduced, and the bridge is described along with the surrounding topography. Here, the monitoring system is also described in detail. Section 3 describes the signal processing and the organization of the data into hierarchical

[1] Postdoc, aksel.fenerci@ntnu.no, ORCID ID: https://orcid.org/0000-0003-1687-5568 , Dept. of Structural Eng., Norwegian University of Science and Technology, Richard Birkelandsvei 1A, 7034 Trondheim, Norway
[2] Postdoc, knut.a.kvale@ntnu.no, ORCID ID: https://orcid.org/0000-0003-2466-3178 , Dept. of Structural Eng., Norwegian University of Science and Technology, Richard Birkelandsvei 1A, 7034 Trondheim, Norway
[3] Postdoc, oyvind.w.petersen@ntnu.no, ORCID ID: https://orcid.org/0000-0003-3563-5041 , Dept. of Structural Eng., Norwegian University of Science and Technology, Richard Birkelandsvei 1A, 7034 Trondheim, Norway
[4] Professor, anders.ronnquist@ntnu.no, ORCID ID: https://orcid.org/0000-0002-9253-4709 , Dept. of Structural Eng., Norwegian University of Science and Technology, Richard Birkelandsvei 1A, 7034 Trondheim, Norway
[5] Professor & Project leader, ole.oiseth@ntnu.no, ORCID ID: https://orcid.org/0000-0002-3746-1842 , Dept. of Structural Eng., Norwegian University of Science and Technology, Richard Birkelandsvei 1A, 7034 Trondheim, Norway

structures. Finally, how the data are stored and organized in the open access repository is explained in Section 4. The paper ends with a short summary.

2. The monitoring campaign

The Hardanger Bridge monitoring campaign started in 2013 shortly after the bridge was opened to traffic and it is still ongoing. The project and the data management were conducted by the Norwegian University of Science and Technology (NTNU) with financial support from the Norwegian Public Roads Administration (NPRA, Statens vegvesen).

2.1. Description of the site

The Hardanger Bridge is spanning the Hardangerfjord which is located at the west coast of Norway. The area is known for its special terrain characterized by steep mountains and wide fjords. The geographical location of the bridge is shown in Figure 1. The bridge lies about 120 km inland from the open sea at the West and is exposed to European windstorms (extratropical cyclones), that produce strong winds along the fjords.

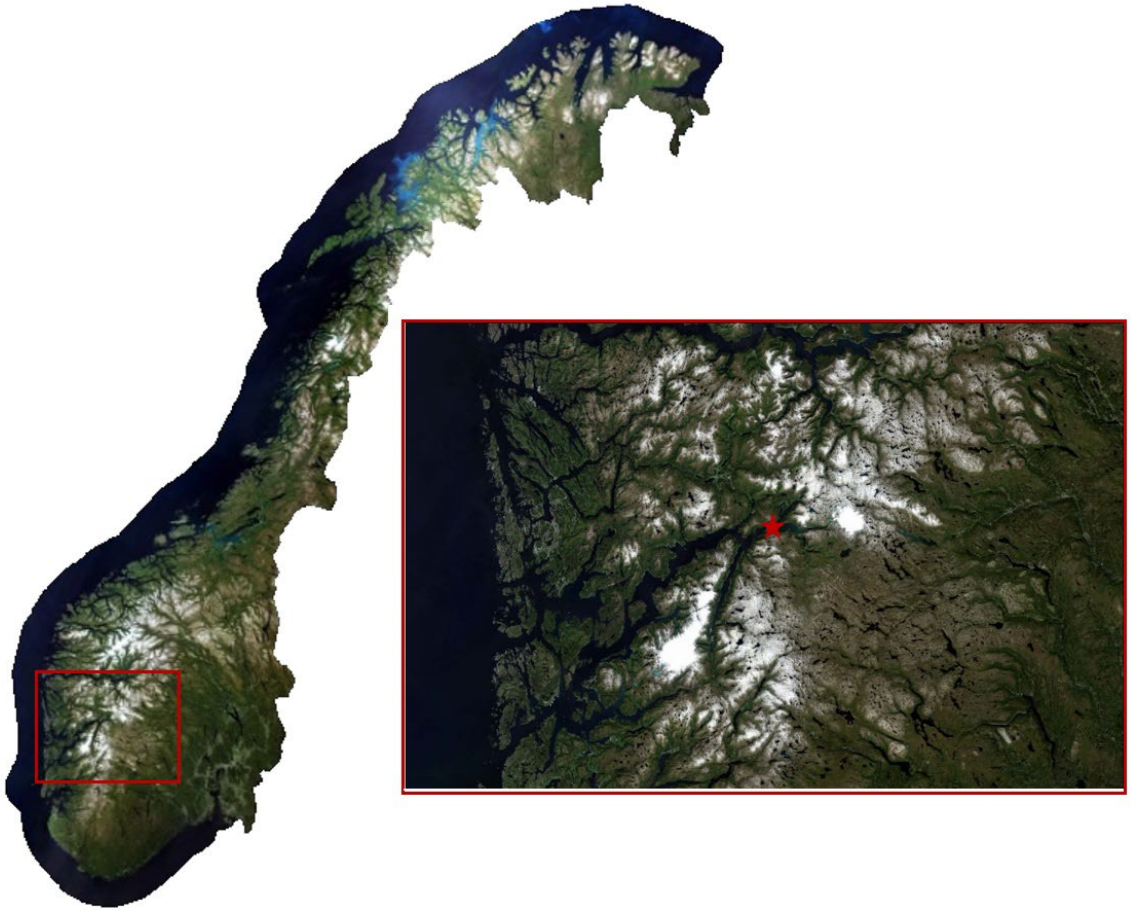

Figure 1 Geographical location of the Hardanger Bridge (the bridge location is indicated by a red star on the zoomed map image). Map image taken from Kartverket©

The local topography surrounding the bridge is especially important for the monitoring campaign since it results in a complicated wind field around the structure. The topographical map of the surroundings of the bridge is shown in Figure 2. The mountains to the north and the south ends of the bridge are

steeply reaching around 1000 meters, where the bridge leads into tunnels on both sides. At the East, the fjord lies almost perpendicular to the bridge and the mountain tops reach about 1600 meters. At the west side, where the fjord divides into two arms, the topography is more complex. The mountains on the east side are taller, and the winds approaching from the North-West are disturbed by the mountainsides.

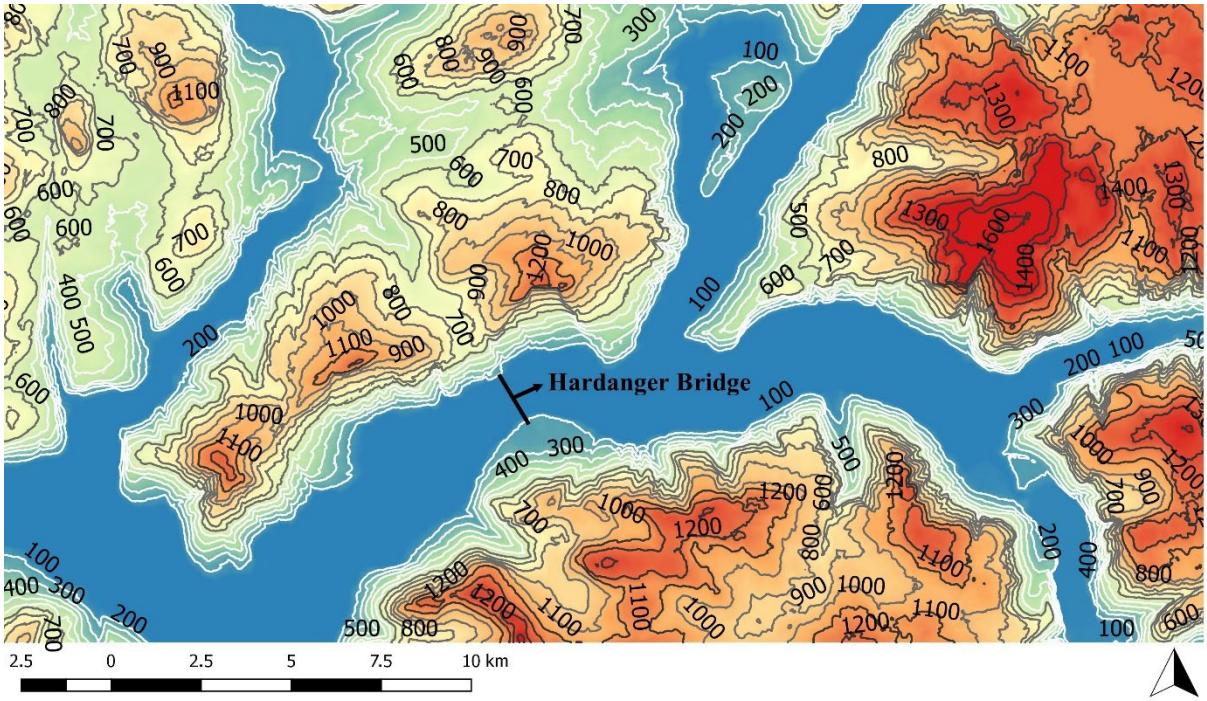

Figure 2 Topographical map of the terrain surrounding the Hardanger Bridge (Map elevation data from Kartverket©)

2.2. The Hardanger Bridge

The Hardanger Bridge is the longest suspension bridge in Norway as of today. It consists of a main span of 1308 meters and two very short side spans connecting to tunnels on both sides Figure 3. As it supports only two traffic lanes and a bicycle line, the bridge is uncommonly slender. The bridge deck is a streamlined steel box deck equipped by guide vanes at the bottom (Figure 4), 3.2 meters high and 18.3 meters wide. The pylons on each side of the slender girder reach to 200 meters. Furthermore, the girder is supported by two main cables and 130 hangers ranging from 2 to 128 meters.

Figure 3 Panorama view of The Hardanger Bridge from the East (Photography by Aksel Fenerci)

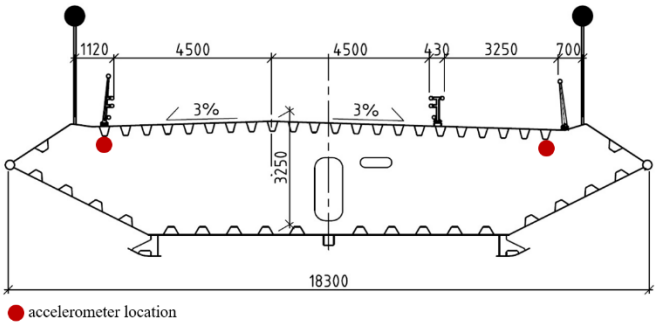

Figure 4 Cross-sectional drawing of the Hardanger Bridge

2.3. The monitoring system

General

The Hardanger Bridge is equipped with an extensive monitoring system that was installed shortly after the bridge was opened to traffic. The monitoring system consists of acceleration and wind sensors (anemometers) for data acquisition, dataloggers for storage, Wi-Fi antennas for data transfer and GPS sensors for time synchronization of the data. Both the data acquisition hardware and the software are developed by Canterbury Seismic Instruments and are commercially available. All sensors are digital, and they are connected to the local loggers by means of ethernet Cat 5 cables. The connection between local loggers and the main logger (Figure 5) is through wi-fi antennas. An overview of the monitoring system is shown in Figure 5 and the sensor coordinates are tabulated in Table 1.

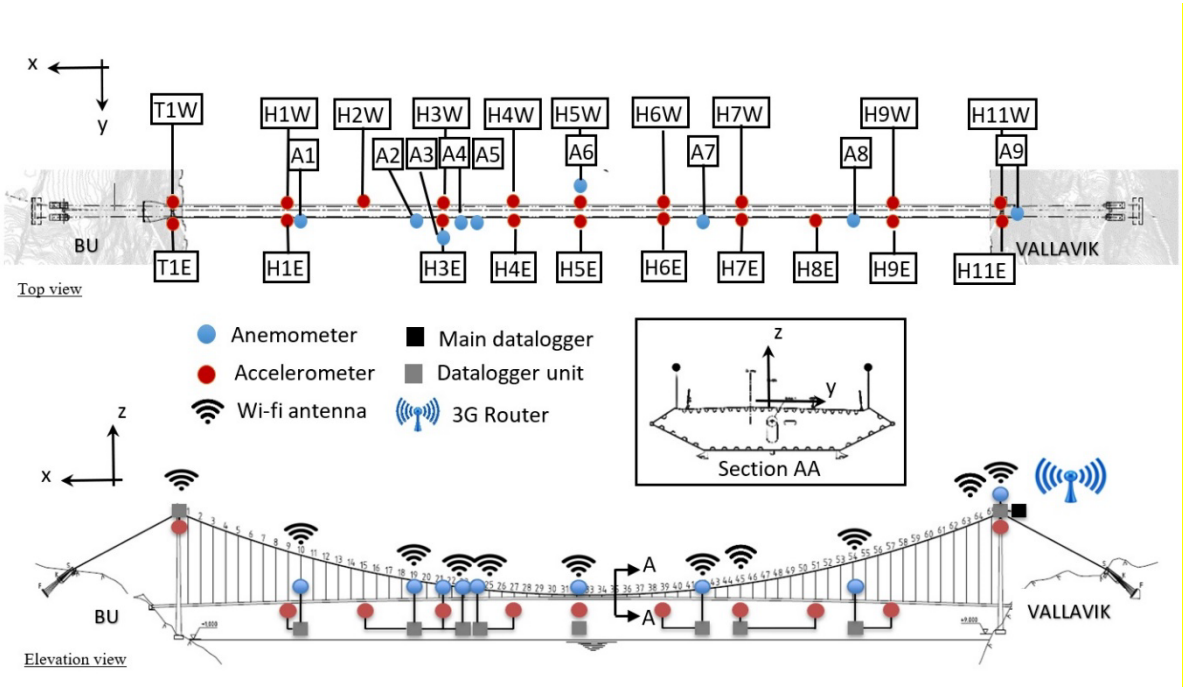

Figure 5 Overview of the monitoring system (20 accelerometers, 9 anemometers, 11 Wi-Fi antennas, 11 GPS sensors, 11 dataloggers)

Table 1 Sensor names and coordinates: the origin of the coordinate system is the midspan of the bridge and positive x-direction points to the south (Bu) end of the bridge

Wind sensors				Accelerometers			
Name	x (m)	y (m)	z (m)	Name	x (m)	y (m)	z (m)
A1	460	7.25	0.3	H1E/H1W	480	6.33/-6.64	-8.38
A2	280	7.25	3.2	H2W	360	-6.64	-6.41
A3	240	7.25	3.9	H3E/H3W	240	6.33/-6.64	-4.45
A4	200	7.25	4.6	H4E/H4W	120	6.33/-6.64	-2.48
A5	180	7.25	4.9	H5E/H5W	-7	6.33/-6.64	-0.4
A6	-10	-7.25	8	H6E/H6W	-120	6.33/-6.64	-2.25
A7	-180	7.25	5.2	H7E/H7W	-240	6.33/-6.64	-4.22
A8	-420	7.25	1.2	H8E	-360	6.33	-6.18
A9	-655	4.5	140	H9E/H9W	-480	6.33/-6.64	-8.15
				H10E/H10W	655	4.5/-4.5	120.5
				H11E/H11W	-655	4.5/-4.5	120.5

Accelerometers

There are 20 accelerometers installed on the bridge. As shown also in Figure 5, these are either located at the tower tops or along the girder. At each tower top, two accelerometers are installed on either side (East & West) of the towers. Along the girder, the accelerometers are also placed on both sides of the girder as pairs to capture the torsional motion of the girder. The exceptions are the accelerometers denoted by H2W and H8E (Figure 5), which do not have pairs. The accelerometers inside the girder are attached to the bulkheads. The precise position is indicated in Figure 4 and pictures of the sensors are shown in Figure 6.

All the accelerometers are CUSP-3D series triaxial accelerographs from Canterbury Seismic Instruments, which are MEMS type accelerometers, characterized with very low noise floor (signal-to-noise ratio of 130 dB according to the manufacturer) and high accuracy at low frequencies. The measurement range of the accelerometers is ±4g where the maximum sampling rate is 200 Hz.

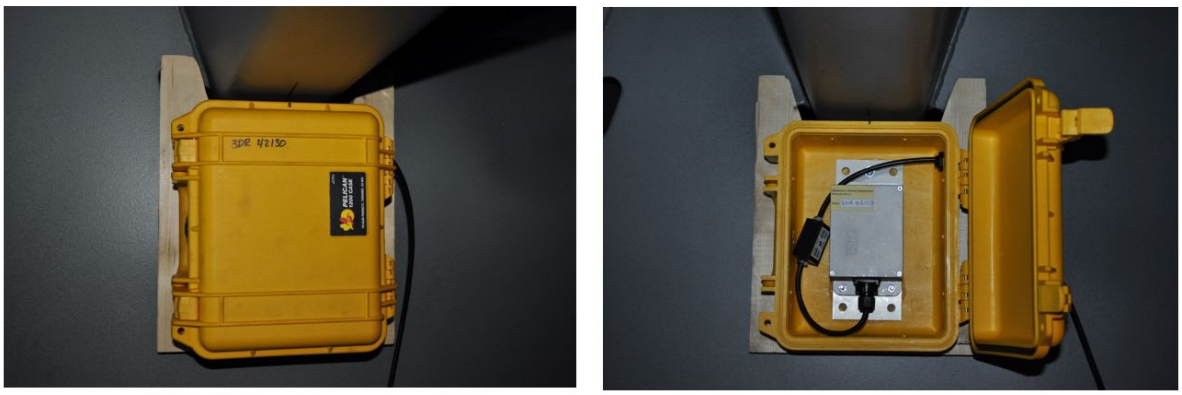

Figure 6 Accelerometers inside the bridge deck

Anemometers

When the monitoring campaign started, the system accommodated 9 anemometers, 8 of which were installed along the span, at a height of 8 meters from the girder to avoid disturbance of the incoming wind flow. The remaining anemometer was installed at the top of the Vallavik (North) tower. However, as of September 2018, this sensor is removed and the wind speeds at the tower tops are no longer measured. This decision was due to lack of useful data acquired during the measurement period. Nevertheless, the data from that sensor that were recorded until its removal will be included in the

dataset described here. As seen in Figure 5, all anemometers except one (A6) along the span are attached to the bridge hangers on the East side of the girder, due to the ease of access provided by the pedestrian lane. The midspan anemometer A6 is installed on the west side to a light pole since the cables at the midspan are too close to the girder and the hangers are too low. Pictures of anemometers are shown in Figure 7.

The anemometers are of the type WindMaster Pros from Gill Instruments. They are 3D ultrasonic anemometers that can measure wind speeds up to 65 m/s with a maximum sampling rate of 32 Hz. In 2016, Gill Instruments announced that some of their anemometers were affected by a software bug that caused errors on the vertical wind measurements (Gill Instruments, 2016). After wind tunnel tests and correspondence with Gill, it is concluded that the anemometers at the Hardanger Bridge were not affected by this bug.

Figure 7 Anemometers on the bridge. On the right side, anemometer A6 is shown, which is attached to a light pole on the West side.

Data Acquisition and storage

When the system is up and running, the sensors measure constantly; however, the data are not recorded unless a threshold wind speed of 15 m/s that is averaged over a one-minute window is not exceeded. If the threshold is exceeded, then a recording of 30 minutes duration is taken. The sensors sample data with the maximum sampling frequency (32 Hz for anemometers and 200 Hz for the accelerometers). After a recording is triggered, the data are recorded on the local dataloggers in the vicinity of the sensors (Figure 8). The data are timestamped using GPS time and resampled internally to a common sample rate of 200 Hz. Data from all loggers are then synced to a main logger unit at the top of the Vallavik tower by means of Wi-Fi communication. There, the data are synced to the servers located at NTNU through an internet connection and stored there permanently.

The GPS sensors and Wi-Fi antennas, which are also attached to bridge hangers, are shown in Figure 9.

Figure 8 Datalogger units. Inside each gray box, there is a datalogger unit, a battery and a charger. The measuring sensors, GPS sensors and Wi-Fi antennas are connected to the logger by wire.

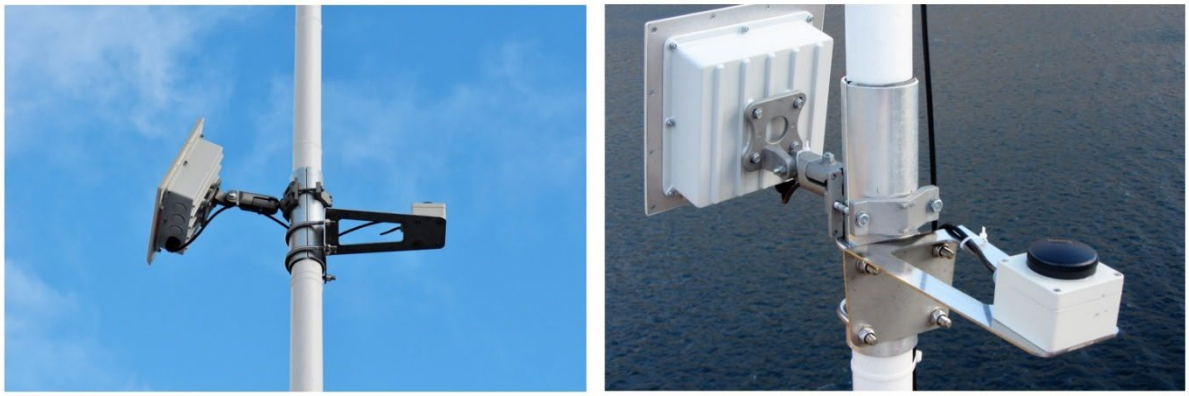

Figure 9 GPS sensors and Wi-Fi antennas. On both pictures, the Wi-Fi antenna is on the left and the GPS sensor is on the right side of the hanger.

3. Organization of the data files

3.1. Raw Data

When a 30-minute recording is completed, the data from all sensors are stored in a single comma-separated-values (.csv) file in tabular format. The name of each file is stamped with the UTC time corresponding to when the recording has started. The naming of the files is shown in Figure 10. Along with the data, the system also generates an XML-file (with .xml extension) that contains the metadata. Here, information about the sensors (type, coordinate axes, serial number, unit, etc.) are listed. A typical CSV-file takes about 110 MB of disk space.

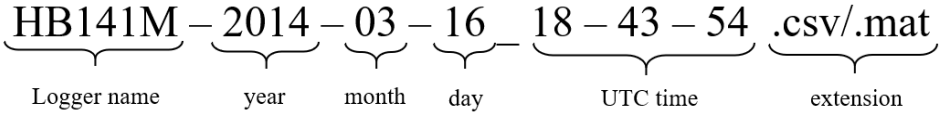

Figure 10 Naming convention for the 30-minute recording files

3.2. Adjusted Data

The data, as they come out of the monitoring system, are not very user-friendly. The amount of data is too large to be dealt with in tabular form. Therefore, some minor adjustments have been made so that the data can be easily accessed and manipulated with the use of common scientific computing software such as MATLAB (The Mathworks, 2019), or Python (Python Software Foundation, 2019). The data are reorganized using MATLAB into v7.3 MAT-files, which are based on the HDF5 file format that allows storage of large datasets in a hierarchical form. In that way, the metadata and numerical data are conveniently stored in a single file. For the new files with. *.mat extension, the same naming convention is used that was shown in Figure 10. The hierarchical structure of an example recording is shown in Figure 11.

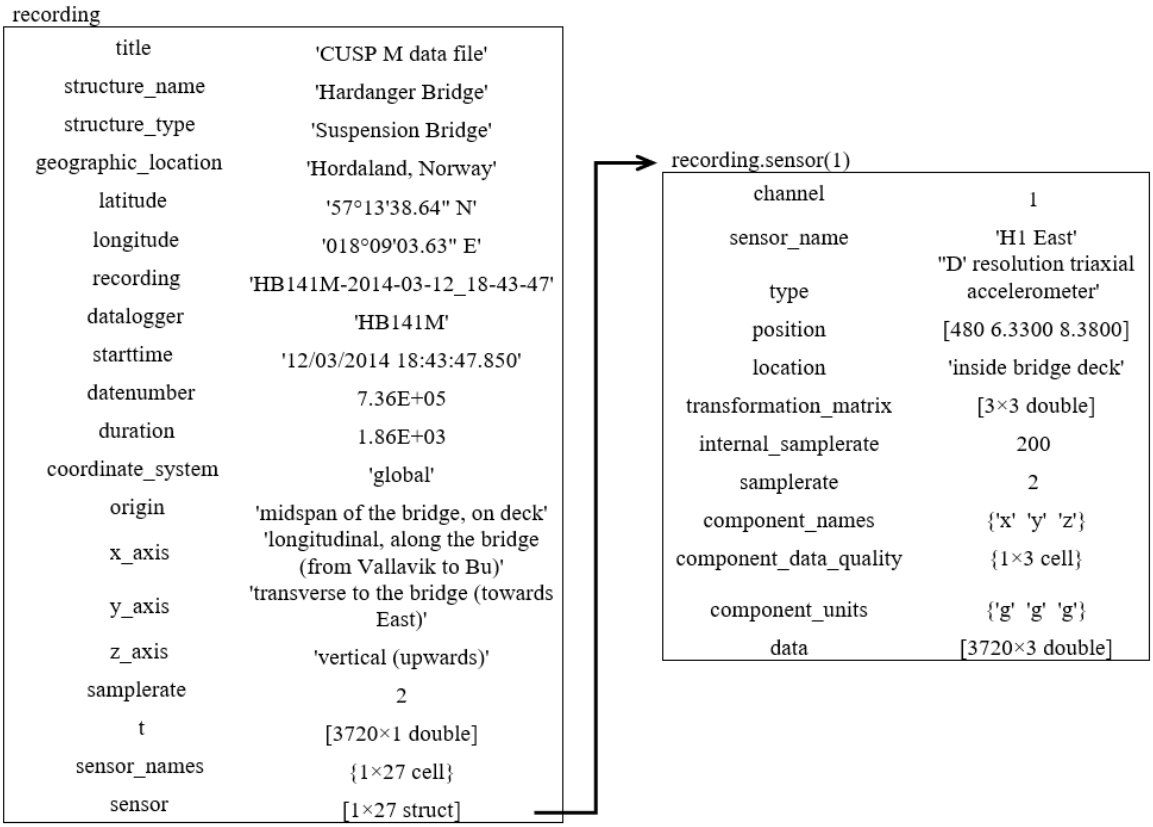

Figure 11 Hierarchical structure of the MAT-files containing adjusted data and metadata

As the data are reorganized, a minimal amount of signal processing is also conducted. Due to the high sampling frequency of the sensors, each data file becomes quite large. For that reason, three different versions of each recording with different sampling rates (2 Hz, 10 Hz and 200 Hz) are created, so that the user can choose the appropriate version depending on the application and avoid the unnecessary burden of downloading and importing large files. The data are resampled using MATLAB, which applies an antialiasing lowpass filter to the signal prior to resampling. The resampling (down sampling) of an example signal is illustrated in Figure 12.

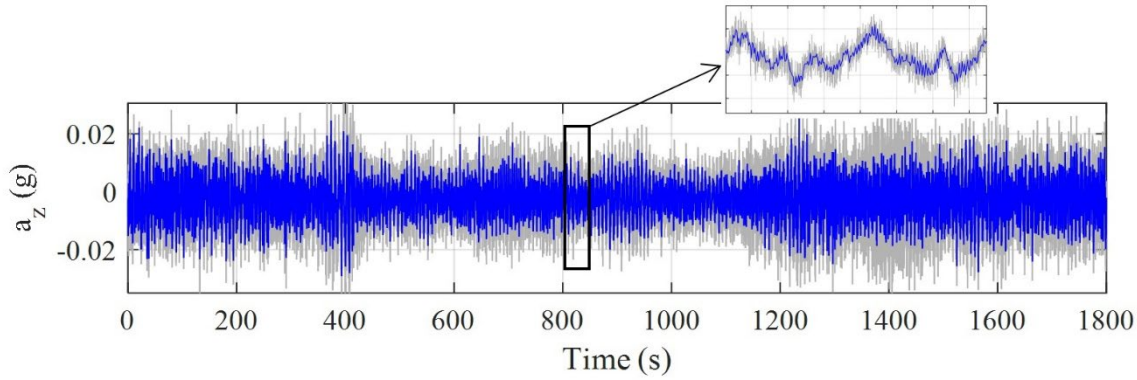

Figure 12 Resampling of a vertical acceleration signal (sensor H8E). The gray lines show the raw data sampled at 200 Hz, where the blue lines are the adjusted data which is resampled to 20 Hz

The signals are also cleared of very large values that indicate errors, when the sensors fail to sample data. To that aim, the data points exceeding 5 times the value of the standard deviation of the signal are removed and replaced with synthetic data by using linear interpolation. Any data point that is outside the measurement range of the sensors is treated in the same way. An example of such processing is shown in Figure 13. The same procedure is applied if the sampled data points are constant for a time window larger than 0.5 seconds, which indicates a temporary dropout of the sensor.

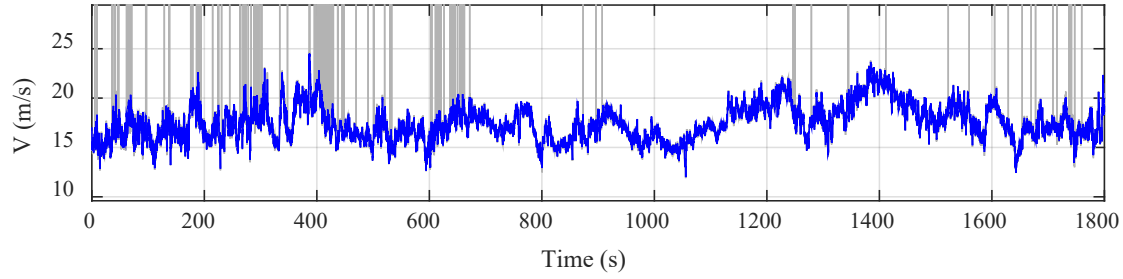

Figure 13 Removing error values from a wind signal (sensor A6). The gray lines show the raw data, where the blue lines are the adjusted data

After the processing, the data are labeled with a quality score. If the data did not require any adjustment, it is labeled as "good" quality. If the adjustments are minor (only a time window smaller than 10 seconds is affected), it is labeled as "acceptable" with the adjustment specified. In case a larger time window than 10 seconds is corrupted, the data quality is labeled as "poor". Then no adjustments are made, and the entire signal is replaced by nan (not-a-number) values. Finally, the data are transformed to the global coordinate system (Figure 5) from the local coordinate systems of the sensors. The data are sampled initially according to the local coordinate systems of the sensors, which are set the same for each type of sensor. The local coordinate systems of anemometers and accelerometers are shown in Figure 14. Since the coordinate systems of the sensors and the global coordinate system are not always coincident, a coordinate transform must be applied to the data. This transformation is done using a transformation matrix as follows:

$$\mathbf{u}_{global}(t) = \mathbf{T}\,\mathbf{u}_{local}(t), \quad \mathbf{u}(t) = [u_1(t), u_2(t), u_3(t)]^T \tag{1.1}$$

where **T** is the transformation matrix, which is also given in the data files for each sensor and for each recording (Figure 11). The transformation matrices can differ between the recordings if the sensor configurations (applies for both physical configuration and data sampling settings) are different. In Table 2, the transformations that were used during the monitoring campaign are listed. Since the cross-terms are always zero, only the diagonals are listed for brevity. It should be noticed that no

transformation was applied to the anemometers, since the local x-axis (0° in polar coordinates) is coincident with the global x axis for all sensors.

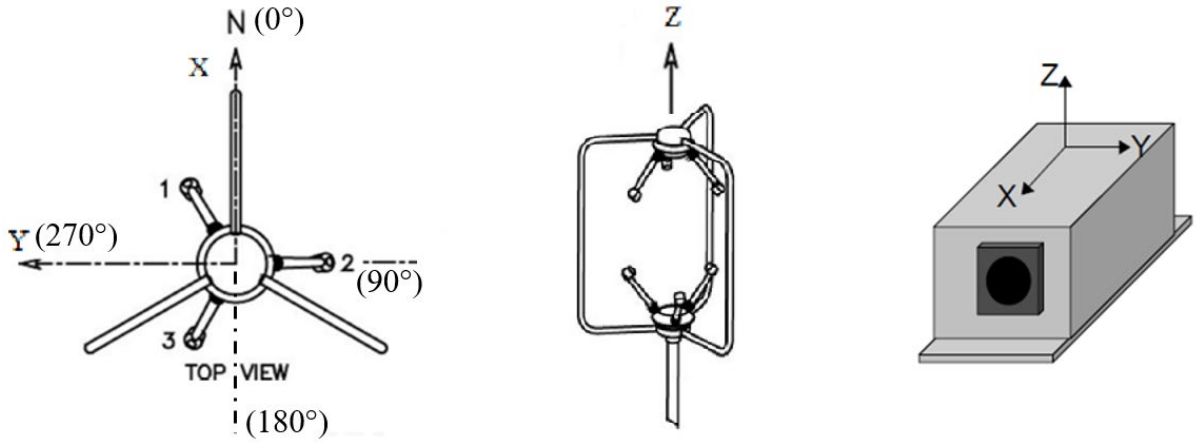

Figure 14 Local coordinate system of the sensors. Left: Anemometer top view. Middle: Anemometer side view. Right: Accelerometer

Table 2 Transformation matrices between local coordinate system of the sensors and the global coordinate system

channel	sensor	diagonal of the T matrix (config 1*)	diagonal of the T matrix (config 2*)	channel	sensor	diagonal of the T matrix (config 1)	diagonal of the T matrix (config 2)
1	H1E	(-1, -1, 1)	(-1, -1, 1)	16	H9W	(1, 1, 1)	(-1, -1, 1)
2	H1W	(-1, -1, 1)	(-1, -1, 1)	17	H10E	(-1, -1, 1)	(1, 1, 1)
3	H2W	(-1, -1, 1)	(-1, -1, 1)	18	H10W	(-1, -1, 1)	(-1, -1, 1)
4	H3E	(-1, -1, 1)	(-1, -1, 1)	19	H11E	(1, 1, 1)	(1, 1, 1)
5	H3W	(-1, -1, 1)	(-1, -1, 1)	20	H11W	(1, 1, 1)	(-1, -1, 1)
6	H4E	(-1, -1, 1)	(-1, -1, 1)	21	A1	(1, 1, 1)	(1, 1, 1)
7	H4W	(-1, -1, 1)	(-1, -1, 1)	22	A2	(1, 1, 1)	(1, 1, 1)
8	H5E	(1, 1, 1)	(-1, -1, 1)	23	A3	(1, 1, 1)	(1, 1, 1)
9	H5W	(1, 1, 1)	(-1, -1, 1)	24	A4	(1, 1, 1)	(1, 1, 1)
10	H6E	(1, 1, 1)	(-1, -1, 1)	25	A5	(1, 1, 1)	(1, 1, 1)
11	H6W	(1, 1, 1)	(-1, -1, 1)	26	A6	(1, 1, 1)	(1, 1, 1)
12	H7E	(1, 1, 1)	(-1, -1, 1)	27	A7	(1, 1, 1)	(1, 1, 1)
13	H7W	(1, 1, 1)	(-1, -1, 1)	28	A8	(1, 1, 1)	(1, 1, 1)
14	H8E	(1, 1, 1)	(-1, -1, 1)	29	A9	(1, 1, 1)	(1, 1, 1)
15	H9E	(1, 1, 1)	(-1, -1, 1)				

*config 1 refers to the sensor configuration before the date 24/10/2015, where config 2 refers to the configuration after that date.

3.3. Missing Data

Throughout the dataset, it is not uncommon that during the time of the recordings one or more sensors were disconnected or were not working. Consequently, some of the recording files have missing sensors. In case of the raw data files in *.csv format, these can be seen from the status columns in the tables. For all sensors that are ordered in the table with the channel number given in Table 2, the status

column reads either "active" or "inactive", the latter of which meaning that the sensor was inactive during the recording and the data are therefore missing. In case of the adjusted data in *.mat file formats, the inactive sensors are simply excluded from the data files. An example of this can be seen in Figure 11, where only 27 sensors are present (instead of the full 29). The remaining sensors can still be tracked by their channel numbers or names, listed in Table 2.

4. Open access dataset

The data described in this paper are published in the open access NTNU BIRD repository. The BIRD platform has been developed by the Unit BIRD consortium for sharing of research data in accordance with Norway's national strategy for accessing and sharing research data. NTNU University Library is one of the consortiums four members. The repository can be accessed with the link:

https://bird.unit.no/

and the database for the Hardanger Bridge Monitoring Project can be accessed via below DOI:

https://doi.org/10.21400/5ng8980s

Alternatively, the dataset can be accessed with the link:

https://bird.unit.no/resources/3e040fe0-dd69-47ca-af8a-683282a2845f/content

where the contents are listed in a more compact manner.

4.1. Organization of the dataset in the repository

Since the size of the data is immense, the data are divided into monthly recordings, which are zipped together. This is done for four versions of the same data:

1. The raw data
2. Adjusted data with original sampling rate (200 Hz & 32 Hz)
3. Adjusted data resampled to 10 Hz
4. Adjusted data resampled to 2 Hz

In that way, the user who is interested in the low-frequency part of the signals (which is usually the case for practical structural engineering applications), can avoid downloading massive amounts of data. Moreover, other small datasets are created, anticipating that the users might be interested only in certain events such as:

1. Storm events
2. Continuous recordings with low wind speed
3. Recordings with highest wind speeds
4. Recordings with highest dynamic response (separate for the drag, lift and pitch responses)

These datasets are available only in the original sampling rate and low sampling rate. The files are named in an organized manner to ease browsing through data. The naming of the zipped files and an overview of all the files in the database in its final status is given in Table 3.

Table 3 Overview of the files in the dataset

description	example	Number of files	Total size (GB)	file format
monthly recordings (raw)	Raw_2015_11	58	761.74	zipped(.csv)
monthly recordings (2 Hz)	LowFreq_2015_11	58	16.77	zipped(.mat)

monthly recordings (10 Hz)	MidFreq_2015_11	58	81.38	zipped(.mat)
monthly recordings (200 Hz)	HighFreq_2015_11	58	895.53	zipped(.mat)
Storm events (2 Hz)	Events_StormTor_LowFreq	5	0.31	zipped(.mat)
Storm events (200 Hz)	Events_StormUrd_HighFreq	5	18.93	zipped(.mat)
Low wind events (2 Hz)	Events_Low_Wind_2015_12_16_LowFreq	8	0.53	zipped(.mat)
Low wind events (200 Hz)	Events_Low_Wind_2015_12_16_HighFreq	8	23.23	zipped(.mat)
Highest wind speed (2 Hz)	Events_Max_Wind_LowFreq	1	0.23	zipped(.mat)
Highest wind speed (200 Hz)	Events_Max_Wind_HighFreq	1	14.72	zipped(.mat)
Highest drag response (2 Hz)	Events_MaxDrag_LowFreq	1	0.02	zipped(.mat)
Highest drag response (200 Hz)	Events_MaxDrag_HighFreq	1	1.44	zipped(.mat)
Highest lift response (2 Hz)	Events_MaxLift_LowFreq	1	0.02	zipped(.mat)
Highest lift response (200 Hz)	Events_MaxLift_HighFreq	1	1.45	zipped(.mat)
Highest pitch response (2 Hz)	Events_MaxPitch_LowFreq	1	0.02	zipped(.mat)
Highest pitch response (200 Hz)	Events_MaxPitch_HighFreq	1	1.38	zipped(.mat)

5. Summary

In this data paper, a large dataset for the Hardanger Bridge monitoring project is introduced. The data acquired during the project are organized and uploaded to the NTNU BIRD platform for research data and made available for download. Since the monitoring project is ongoing, the database might be updated with new data in the future. This will be achieved by publishing new versions of the database. The DOI given in this paper will be permanently linked to the database and will direct the user to the latest version of the data. The version history will be visible on the repository and previous versions will be also reachable.

6. Acknowledgements

The research project that produced the data described here is financially supported by the Norwegian Public Roads Administration (Statens vegvesen). NTNU's instance of the BIRD repository used in publication of the data is financed and maintained by the NTNU University Library. The authors also thank Sven K. Strøm and Ingrid Heggland from the NTNU University Library for their assistance in publication of the data.

7. References

Fenerci, Aksel, Øiseth, O., 2018. Site-specific data-driven probabilistic wind field modeling for the wind-induced response prediction of cable-supported bridges. J. Wind Eng. Ind. Aerodyn. 181, 161–179. https://doi.org/https://doi.org/10.1016/j.jweia.2018.09.002

Fenerci, A., Øiseth, O., 2018. Strong wind characteristics and dynamic response of a long-span suspension bridge during a storm. J. Wind Eng. Ind. Aerodyn. 172. https://doi.org/10.1016/j.jweia.2017.10.030

Fenerci, A., Øiseth, O., 2017a. Evaluation of wind-induced response predictions of a long-span suspension bridge using full-scale measurements, in: 7th European and African Conference on Wind Engineering (EACWE 2017), Liege, Belgium.

Fenerci, A., Øiseth, O., 2017b. Measured Buffeting Response of a Long-Span Suspension Bridge Compared with Numerical Predictions Based on Design Wind Spectra. J. Struct. Eng. (United States). https://doi.org/10.1061/(ASCE)ST.1943-541X.0001873

Fenerci, A., Øiseth, O., 2017c. The Hardanger Bridge monitoring project: Long-term monitoring results and implications on bridge design. Procedia Eng. 199, 3115–3120. https://doi.org/https://doi.org/10.1016/j.proeng.2017.09.576

Fenerci, A., Øiseth, O., Rønnquist, A., 2017. Long-term monitoring of wind field characteristics and dynamic response of a long-span suspension bridge in complex terrain. Eng. Struct. 147, 269–284. https://doi.org/10.1016/j.engstruct.2017.05.070

Gill Instruments, 2016. Software bug affecting 'w' wind component of the WindMaster family.

Lystad, T.M., Fenerci, A., Øiseth, O., 2020. Buffeting response of long-span bridges considering uncertain turbulence parameters using the environmental contour method. Submitted.

Lystad, T.M., Fenerci, A., Øiseth, O., 2019. Aerodynamic Effect of Non-uniform Wind Profiles for Long-Span Bridges BT - Proceedings of the XV Conference of the Italian Association for Wind Engineering, in: Ricciardelli, F., Avossa, A.M. (Eds.), . Springer International Publishing, Cham, pp. 427–439.

Lystad, T.M., Fenerci, A., Øiseth, O., 2018. Evaluation of mast measurements and wind tunnel terrain models to describe spatially variable wind field characteristics for long-span bridge design. J. Wind Eng. Ind. Aerodyn. https://doi.org/10.1016/j.jweia.2018.06.021

Petersen, Ø.W., Øiseth, O., 2017. Finite element model updating of a long span suspension bridge, in: The International Conference on Earthquake Engineering and Structural Dynamics, Reykjavik, Iceland.

Petersen, Ø.W., Øiseth, O., Lourens, E., 2020. Investigation of dynamic wind loads on a long-span suspension bridge identified from measured acceleration data. J. Wind Eng. Ind. Aerodyn. 196, 104045. https://doi.org/https://doi.org/10.1016/j.jweia.2019.104045

Petersen, Ø.W., Øiseth, O., Lourens, E.M., 2019. The use of inverse methods for response estimation of long-span suspension bridges with uncertain wind loading conditions: Practical implementation and results for the Hardanger Bridge. J. Civ. Struct. Heal. Monit. https://doi.org/10.1007/s13349-018-0319-y

Petersen, Ø.W., Øiseth, O., Lourens, E.M., 2017. Estimation of the dynamic response of a slender suspension bridge using measured acceleration data, in: Procedia Engineering. https://doi.org/10.1016/j.proeng.2017.09.547

Python Software Foundation, 2019. Python 3.7.4 documentation [WWW Document]. Jul 17, 2019.

The Mathworks, I., 2019. MATLAB, Version 9.6. www.mathworks.com/products/matlab.